Altering the Reaction Specificity of Eukaryotic Ornithine Decarboxylase[†,‡]

Laurie K. Jackson,[§] Harold B. Brooks,[§,||] Andrei L. Osterman,[§,⊥] Elizabeth J. Goldsmith,[#] and Margaret A. Phillips*[,§]

Department of Pharmacology and Department of Biochemistry, The University of Texas Southwestern Medical Center at Dallas, 5323 Harry Hines Boulevard, Dallas, Texas 75390-9041

Received May 26, 2000; Revised Manuscript Received July 14, 2000

ABSTRACT: Ornithine decarboxylase (ODC) catalyzes the first committed step in the biosynthesis of polyamines, and it has been identified as a drug target for the treatment of African sleeping sickness, caused by *Trypanosoma brucei*. ODC is a pyridoxal 5′-phosphate (PLP) dependent enzyme and an obligate homodimer. X-ray structural analysis of the complex of the *T. brucei* wild-type enzyme with the product putrescine reveals two structural changes that occur upon ligand binding: Lys-69 is displaced by putrescine and forms new interactions with Glu-94 and Asp-88, and the side chain of Cys-360 rotates into the active site to within 3.4 Å of the imine bond. Mutation of Cys-360 to Ala or Ser reduces the k_{cat} of the decarboxylation reaction by 50- and 1000-fold, respectively. However, HPLC analysis of the products demonstrates that the mutant enzymes almost exclusively catalyze a decarboxylation-dependent transamination reaction to form pyridoxamine 5-phosphate (PMP) and γ-aminobutyraldehyde, instead of PLP and putrescine. This side reaction arises when the decarboxylated substrate intermediate is protonated at C4′ of PLP instead of at the C_α of substrate. For the reaction catalyzed by the wild-type enzyme, this side reaction occurs infrequently (<0.01% of the turnovers). Single turnover analysis and multiwavelength stopped-flow spectroscopic studies suggest that for the mutant ODCs protonation at C4′ occurs either very rapidly or in a concerted reaction with decarboxylation and that the rate-limiting step in the steady-state reaction is Schiff base hydrolysis/product release. These studies demonstrate a role for Cys-360 in the control of the C_α protonation step that catalyzes the formation of the physiological product putrescine. The results further provide insight into the mechanism by which this class of PLP-dependent enzymes controls reaction specificity.

Ornithine decarboxylase (ODC)[1] is a pyridoxal 5′-phosphate (PLP) dependent enzyme that catalyzes the formation of the polyamine putrescine, an essential and ubiquitous cell growth factor (*1*). ODC has been studied as a drug target for the treatment of a number of proliferative diseases, a point illustrated by the finding that α-difluoromethylornithine (DFMO), a suicide inhibitor of ODC, cures African sleeping sickness and is now used clinically for treatment of the disease (*2*, *3*).

PLP-dependent enzymes catalyze a wide range of reaction chemistry involving amino acids, including decarboxylation, transamination, racemization, β- or γ-elimination, and carbon−carbon bond formation (*4*). Five separate structural classes of PLP-dependent enzymes have been identified (*5*). All enzymes that utilize PLP in a catalytic role bind the cofactor via a Schiff base to an active site Lys residue (Lys-69 in ODC). Substrate displaces the Lys residue in a transimination reaction to form the external aldimine species (Figure 1). Formation of this species allows the cofactor to serve as an electron sink to stabilize the carbanion generated by cleavage of one of three bonds to the C_α-carbon. Reaction specificity is dictated by the specific nature of the enzyme active site. For example, the C_α−carboxylate bond is cleaved by decarboxylases, and the C_α−proton bond is cleaved by transaminases and racemases. In the second step of these reactions, protonation occurs at C_α (decarboxylation and racemization) or at C4′(transamination) depending on the reaction chemistry.

To control the reaction specificity, the enzyme promotes the physiologically productive reaction while limiting the vast array of potential side reactions. The fidelity of the reaction chemistry has been studied in a number of PLP-dependent enzymes. For the decarboxylases, studies on methionine (*6*, *7*) and glutamate (*8*) decarboxylase found that decarboxylation-dependent transamination occurs as a rare side reaction with the physiological substrates (1 time in 10^4 catalytic events), while it occurs more frequently with nonphysiological substrates (e.g., for 2-methylglutamate 1% of the product

[†] This work was supported by grants (to M.A.P.) from the National Institutes of Health (R01AI34432), the Welch Foundation (I-1257), and the American Heart Foundation, (to L.K.J.) from the National Institutes of Health (T32GM07062), (to H.B.B.) from the National Institutes of Health (F32AI09495), and (to E.J.G.) from the Welch Foundation I-1128. M.A.P. is a recipient of a Burroughs Wellcome Fund Scholar Award in Molecular Parasitology.

[‡] Coordinates for the structures of *T. brucei* ODC bound to putrescine have been deposited in the protein database with the PDB ID code 1f3t.

* To whom correspondence should be addressed. Tel: (214) 648-3637. Fax: (214) 648-9961. E-mail: philli01@utsw.swmed.edu.

[§] Department of Pharmacology.

[||] Present address: Eli Lilly Co., Lilly Corporate Center, Indianapolis, IN 46285.

[⊥] Present address: Integrated Genomics Inc., 2201 W. Campbell Park Dr., Chicago, IL 60612.

[#] Department of Biochemistry.

[1] Abbreviations: ODC, ornithine decarboxylase; C360A ODC, *T. brucei* ODC mutant with Ala replacing Cys at position 360; C360S ODC, *T. brucei* ODC mutant with Ser replacing Cys at position 360; PLP, pyridoxal 5′-phosphate; PMP, pyridoxamine 5′-phosphate; DFMO, α-difluoromethylornithine; Orn, L-ornithine; Put, putrescine; Pyr, pyrrolidine; γABA, γ-aminobutyraldehyde.

10.1021/bi001209s CCC: $19.00
Published on Web 08/22/2000

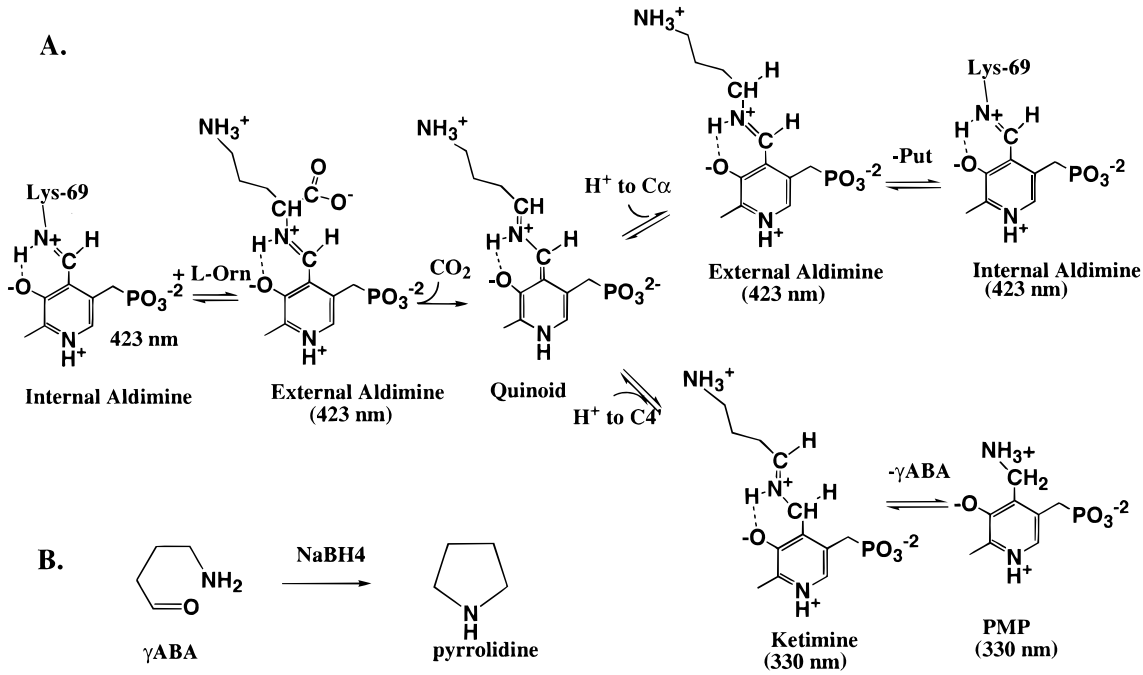

FIGURE 1: (A) Reaction mechanism for ODC. Protonation at C_α leads to formation of the physiological product, putrescine, while protonation at C4′ leads to transamination to form PMP and γABA. (B) Reduction of γABA produces pyrrolidine. The spectral properties of the PLP intermediates were taken from (*10*, *33*) and represent the major band observed at pH 7.5.

is incorrectly protonated by glutamate decarboxylase). This reaction, which converts the active PLP cofactor into an inactive form, PMP, occurs if the quinoid that is generated upon decarboxylation is protonated at C4′ instead of C_α (Figure 1). Dunathan proposed that PLP-dependent enzymes control the bond cleavage step by orienting the scissile bond perpendicular to the plane of the π electrons of the imine bond with PLP (*9*). Less is known about how these enzymes control the specificity of the protonation step. The proper positioning of a general acid and/or the exclusion of water from inappropriate positions in the active site are potential mechanisms for controlling the selectivity of this step.

The reaction mechanism of ODC has been studied by stopped-flow multiwavelength spectroscopy (*10*). Formation of the external aldimine is followed by decarboxylation to generate a putative quinoid intermediate that is protonated on the C_α-carbon to produce the product putrescine (Figure 1). Product release, which includes Schiff base hydrolysis, has been identified as the likely rate-determining step in the reaction. The X-ray structures of ODC from several eukaryotic sources [mouse (*11*), *T. brucei* (*12*), and human (*13*)] have recently been solved, and the catalytic roles of a number of the active site residues have been delineated (*14*−*16*). Cys-360 was identified as the nucleophile that is labeled by the mechanism-based inhibitor DFMO (*17*). Further mutation of Cys-360 to Ala in both mouse (*18*, *19*) and *T. brucei* (*20*) ODC decreases the steady-state k_{cat} for decarboxylation of L-Orn. Comparison of the X-ray structures of unliganded ODC with the DFMO-bound enzyme shows that the side chain of Cys-360 points away from the active site in the unliganded enzyme; however, upon reaction with DFMO, the side chain rotates 145°, positioning the sulfur group to within 4 Å of the C_α carbon. These data suggested that Cys-360 plays a role in the reaction chemistry of the enzyme.

In this paper, we demonstrate that substitution of Cys-360 with either Ala or Ser alters the reaction specificity of *T. brucei* ODC. Both mutant enzymes catalyze decarboxylation-dependent transamination as the primary reaction. The k_{cat} for steady-state decarboxylation has been reduced by 50- and 1000-fold for C360A and C360S ODC. Single-turnover experiments demonstrate that the rate of the decarboxylation step is also decreased by these mutations, but to a lesser extent than k_{cat}. The rate-limiting step in the steady-state reaction is Schiff base hydrolysis/product release to form γ-aminobutyraldehyde (γABA) and PMP. X-ray analysis of wild-type *T. brucei* ODC in complex with putrescine demonstrates that rotation of the Cys-360 side chain into the active site occurs upon ligand binding and it does not depend on the formation of a covalent bond between Cys-360 and DFMO. These data demonstrate that Cys-360 is positioned to play a role in the reaction chemistry and that this role is essential for formation of the physiological product.

EXPERIMENTAL PROCEDURES

Materials

HPLC grade acetonitrile, trifluoroacetic acid, amino acids, amines, buffers, PLP, PMP, and pyrrolidine were purchased from Sigma. Ni^{2+}−agarose was purchased from Qiagen. Centricon concentrators were purchased from Amicon. 1-$^{14}CO_2$-L-Orn (56 mCi/mmol, 0.02 mM) was obtained from Amersham.

Methods

Site-Directed Mutagenesis, ODC Expression, and Purification. The construction of the clone encoding C360A *T. brucei* ODC has been previously described (*20*). The clone encoding C360S *T. brucei* ODC was created by standard Kunkel mutagenesis (*21*) using the oligo 5′-GGGGTCCCACTAGTGATGGTCTTG-3′ to substitute the codon for Ser (underlined) at position 360 and to introduce a silent *Spe*I site. Wild-type and mutant ODCs were expressed from the cloned gene as His-tag fusion proteins in BL21/DE3 cells,

Table 1: X-ray Structure Parameters for *T. brucei* ODC Bound to Putrescine

A. Data Collection and Processing	
data source	Beamline 5.0.2 at ALS
wavelength (Å)	1.10
temperature (K)	124
resolution (Å)	20.0−2.0
total reflections	402763
unique reflections	111865
completeness (%) (last shell $I > \sigma$)	99.3 (96.8)
multiplicity	3.6
intensities $I > \sigma$ (last shell)	19.9 (3.2)
R_{merge}	0.07
B. Refinement	
no. of reflections ($F > 0\sigma$)	104951 (8−2.0 Å)
no. of non-H protein atoms	11737
no. of water molecules	380
$R_{crystal}$ (%)/R_{free} (%) ($F > 0\sigma$)	23.7/28.0 (8−2.0 Å)
RMSD bonds	0.01
RMSD bond angles	1.5
average *B*-values (Å^2)	29.6
B rmsd for bonded main-chain atoms	2.61
B rmsd for bonded side-chain atoms	3.58

from the T7 promoter. The enzyme for kinetic analysis and for crystallization was purified by Ni^{2+}−agarose column chromatography and gel filtration as previously described (*10*). Protein for crystallization was further purified by removal of the His-tag as described (*22*). The buffer in the protein samples was exchanged with 0.1 M Hepes, pH 7.5, using a Fast Desalting HR 10/10 column (Pharmacia) equilibrated in the same buffer prior to use in kinetic studies. The protein concentration in all ODC samples was determined by absorbance spectroscopy using a previously determined extinction coefficient of $\epsilon = 0.85$ OD (mg/mL)$^{-1}$ cm^{-1} (*20*).

Crystallization. The putrescine-complexed crystals were prepared as follows: ODC (25 mg/mL ODC in 10 mM Hepes, pH 7.2, 50 mM NaCl, 10 mM DTT, 0.5 mM EDTA, 0.01% Brij-20) was preincubated with D-Orn (15 mM), pH 7.5, for 10 min at room temperature before crystallization. The crystals were obtained at 16 °C by vapor diffusion, mixing equal volumes of ODC−D-Orn mixture and well solution (20% PEG 3350, 0.2 M NaOAc, 100 mM Hepes, pH 7.5, 10 mM DTT). This procedure resulted in mostly twinned crystals that were used for microseeding into sitting drops containing the solution described above. Most crystals grew in clusters and were twinned. However, a few single crystals were located near the edges of the drop. Crystallographic analysis indicated that the D-Orn was decarboxylated into putrescine; thus, the final structure represents ODC bound to putrescine. Samples were cryo-protected and frozen in liquid nitrogen as described previously (*22*).

Data Collection and Processing. Diffraction data were collected at 124 K on beam line 5.0.2 at the Advanced Light Source (ALS, Berkeley). Data were processed and scaled using DENZO and SCALEPACK (*23*). A summary of the data processing statistics is given in Table 1.

Structure Determination and Refinement. Initial phases were calculated from a molecular replacement [program AMoRe (*24*)] solution obtained using the *T. brucei* ODC K69A/DFMO structure (pdb accession no. 2tod) as the search model, where DFMO was removed from the structure (*12*). The model was built in O (*25*). The structure was refined with CNS (*26*−*28*) using molecular dynamics and energy minimization on data between 8 and 2.0 Å. Once R_{free} was below 35%, individual *B*-factors were refined. Tight noncrystallographic symmetry constraints were kept for the four monomers in the asymmetric unit until the last cycles of the refinement. Relaxation of this restraint yielded only slight structural changes. The peptide torsion angles for 1110 out of 1246 well-defined nonglycine and nonproline residues fall within the most favored regions of the Ramachandran plot, as defined in the program PROCHECK (*29*). There are no residues in disallowed regions.

pH Dependence of the Spectra of PLP Bound to C360A and C360S ODC. Spectra of C360A and C360S ODC (30 μM) were recorded on a Beckman DU-650 spectrophotometer over a pH range of 7−9 using 0.1 M $NaPO_4$ (pH 6.5−6.75), Hepes (pH 7−8), or Bicine (pH 8.25−9) buffers as described (*16*). To account for the contribution of unbound PLP, the sample was subjected to ultrafiltration using Centricon-10 units (Amicon). The flow-through for every sample was collected, and the spectra were recorded and subtracted from the corresponding initial spectra. The spectra were recalculated to millimolar absorptivities.

The minimal model that describes the spectral pH titration data for C360A or C360S ODC requires a cooperative $2H^+$ dissociation. Millimolar absorptivities observed at 420 nm (ϵ_{obs}^{420nm}) were fitted to eq 1, which describes the interconversion of the two spectrally distinct forms (E and EH_2), having extinction coefficients of ϵ_E^{420nm} and ϵ_{EH}^{420nm}.

$$\epsilon_{obs}^{420nm} = \epsilon_{EH}^{420nm}\frac{[H^+]^2}{K_a^2 + [H^+]^2} + \epsilon_E^{420nm}\frac{K_a^2}{K_a^2 + [H^+]^2} \quad (1)$$

Like wild-type ODC, significant loss of PLP from the active sites of C360A or C360S ODC did not occur until the pH was above 9.0.

Steady-State Analysis of the Reaction of L-*Orn with ODC by Determination of CO_2 Production.* Decarboxylation was followed at 37 °C using a modification of the previously described spectrophotometric assay where CO_2 production is coupled to NADH oxidation via phosphoenolpyruvate carboxylase and malate dehydrogenase (*20*). The following reaction conditions were used: 0.1 M Hepes−NaOH, pH 7.5, 0.32 mM NADH, 2.2 mM phosphoenolpyruvate, 10 mM $MgCl_2$, 2 mM DTT, 0.05−0.2 mM PLP, 0.25−10.0 mM L-Orn, 10% reagent B (Sigma CO_2 detection kit 132-B which contains 2.5 units/mL plant phosphoenolpyruvate carboxylase and 15 units/mL porcine heart malate dehydrogenase), and ODC (wild-type ODC, 5−50 nM; C360A ODC, 1−4 μM; C360S ODC, 2−10 μM) in a final volume of 0.5 mL. Absorbance units were converted to moles of CO_2 produced based on the extinction coefficient of NADH (6.2 mM^{-1} cm^{-1}) and the assumption that 1 mol of CO_2 is produced for every mole of NADH oxidized.

Single Turnover Kinetic Analysis of the Reactions of ODC with L-*Orn.* Single turnover data were collected under conditions in which the concentration of ODC (0.05−1.1 mM) was in excess over the concentration of 1-$^{14}CO_2$-L-Orn (17 μM). At various time points, the reaction was quenched with NaOH (1 M) and cold L-Orn (25 mM). $^{14}CO_2$ was driven from solution by acidification (6 M HCl), and the unreacted 1-$^{14}CO_2$-L-Orn was quantitated by scintillation counting. This method was used previously to monitor

Scheme 1

$$E + S \underset{k_{off.Orn}}{\overset{k_{on.Orn}}{\rightleftharpoons}} ES \xrightarrow{k_{decarb}} EP$$

the decarboxylation rate for K69A ODC (*14*); however, because this mutant enzyme catalyzed the reaction very slowly, rapid mixing protocols were not required. For wild-type, C360A, and C360S ODC, the reaction occurred fast, and quenching was performed in an SFM4 mixer (Biologic, France) equipped with a quench-flow exit valve, no delay line in DL1, and a 0.09 mL delay line in DL2. The exact mixing protocol was as follows. The four syringes are set up with the following reaction components: syringe 1 (S1; 100 mM Hepes, pH 7.5); syringe 2 (S2; 0.1−2.2 mM ODC in 100 mM Hepes, pH 7.5); syringe 3 (S3; 34 μM, 1.7 μCi/mL, 1-$^{14}CO_2$-L-Orn diluted in 0.1 M Hepes, pH 7.5); and syringe 4 (S4, 2 M NaOH with 50 mM L-Orn). The mixer is purged with 0.2 mL from S1, 0.05 mL from S2, and 0.05 mL from S3, followed by 0.7 mL from S1. This mixture is discarded. After 2.5 s, which allows for the collection tube to be positioned, the mixer is primed with 0.024 mL of ODC from S2, and the reaction is initiated with 0.054 mL from both S2 (ODC) and S3 (1-$^{14}CO_2$-L-Orn). After the sample is allowed to age, the reaction is collected by expelling with 0.34 mL of buffer from S1 and quenched with 0.34 mL from S4 (NaOH and L-Orn). Aging times were obtained using interrupted flow.

The decay of $^{14}CO_2$ from solution under single turnover conditions (e.g., [E] ≫ [S]) follows first-order kinetics, and the data were fitted to eq 2A to obtain k_{obs} (the observed first-order rate constant for the decarboxylation of L-Orn), where b is an offset to account for a nonzero baseline.

$$[Orn] = [Orn]_o e^{-k_{obs}t} + b \tag{2a}$$

The k_{obs} data were fitted to eq 2B (*30*), which describes a one-step binding model (Scheme 1), followed by an irreversible decarboxylation step. E represents free enzyme, ES and EP are the Schiff base species with substrate and product, respectively, E_T is the total concentration of ODC in the reaction, k_{decarb} is the first-order rate constant for the chemical conversion (decarboxylation), and $K_{m.decarb}$ is the Michaelis constant for the steps up to decarboxylation.

$$k_{obs} = \frac{k_{decarb}[E_T]}{K_{m.decarb} + [E_T]} \tag{2b}$$

Pre-Steady-State Kinetic Analysis of the Reaction of L-*Orn with ODC by Multiwavelength Stopped-Flow Spectroscopy.* The pre-steady-state kinetics of C360A and C360S ODC reacting with L-Orn were monitored using a Biologic SFM3 mixer equipped with a TC-100 quartz cell (path length of 1 cm) coupled to a J&M Tidas16 256 diode array for multiwavelength data collection (Molecular Kinetics, Pullman, WA). The SFM3 using the TC-100 cell has a dead time of 3 ms with a flow velocity of 12 mL/s. The diode array has a spectral acquisition time of 0.8 ms at a wavelength resolution of 2.1 nm over a range of 190−730 nm. The mixer parameters and reaction setup were as previously described (*10*). The final mixtures contained L-Orn (10 mM), ODC (0.12 mM ODC), and buffer (0.1 M Hepes, pH 7.5). Multiwavelength data were collected from 310 to 500 nm over 3−60 000 ms. A typical collection regime is as follows: a spectrum was collected every 1 ms for the first 250 ms, every 50 ms for the next 10 s, and every 1000 ms for the final 60 s.

Scheme 2

$$A \xrightarrow{k_{obs1}} B \xrightarrow{k_{obs2}} C \xrightarrow{k_{obs3}} D$$

Multiwavelength data were analyzed using Specfit 2.12 (Spectrum Software Associates, Chapel Hill, NC) which uses singular value decomposition (SVD analysis) to solve for the spectral eigenvectors (*31*). The eigenvectors were then used to reconstruct the spectra of chemical species and their kinetics using a model-dependent multivariate least-squares implementation of the Levenberg−Marquardt algorithm (*32*). The data for C360A and C360S ODC were fitted to a three-step model (Scheme 2).

Steady-State Analysis of the Reaction of L-*Orn with ODC by Chromatographic Determination (HPLC) of Product Formation.* ODC (0.5 μM for wild-type ODC, 2.5 μM for C360A ODC, and 4.5 μM for C360S ODC) was incubated with L-Orn (2 mM) and PLP (0.2−2 mM) in buffer (15 mM potassium phosphate, pH 7.4, containing 1 mM DTT) for a range of times (60−8000 s) at 37 °C. The reactions were stopped by the addition of TCA (final concentration of 4%). Cadaverine (final concentration 0.15−0.3 mM) was added as an internal standard. An aliquot of the sample was treated with $NaBH_4$ (10 mg/mL for 5 min at ambient temperature). Aliquots (2−4 μmol) of both the $NaBH_4$-treated and the untreated samples were derivatized using the AccQ·TAG kit (Waters, Milford, MA). Derivatized ligand was analyzed by HPLC on an AccQ·TAG column equilibrated with buffer A (140 mM sodium acetate, 17 mM triethylamine, pH 5.1) and eluted with the following gradient: 0 min, 0% B; 1 min, 5% B; 10 min, 30% B; 35 min, 100% B; where B is 60% acetonitrile. The column was calibrated using the retention times (RT) of the following standards (25−100 pmol) derivatized as above: L-Orn (RT = 13.3 min), putrescine (RT = 19.0 min), cadaverine (RT = 21.2 min), pyrrolidine (RT = 15.6 min), PMP (RT = 13.0 min). The concentration of putrescine, pyrrolidine, and PMP in the analyzed samples was determined from a standard curve generated from known concentrations of the compounds, with respect to the internal standard. A conversion factor for γABA was generated assuming 1 mol of γABA is converted to 1 mol of pyrrolidine upon reduction. Rates of product formation (putrescine, pyrrolidine, γABA, or PMP) were calculated from reaction mixtures in which <25% of the PLP and L-Orn were consumed.

For wild-type ODC, the transamination rate was determined by following the decrease in absorbance at 420 nm. Data were collected in 0.1 mM Hepes, pH 7.5, over a time range of 2−3 min after mixing L-Orn (250 mM) with ODC (25 μM). The steady-state rate was estimated from the initial rate phase of the curve. Absorbance units of PLP were converted to moles using the extinction coefficient for PLP (4.4 mM^{-1} cm^{-1} at 420 nm).

RESULTS

X-ray Structure Analysis of Wild-Type T. brucei ODC Bound to Putrescine. Previously we reported the X-ray structures of native *T. brucei* ODC and of the *T. brucei* ODC

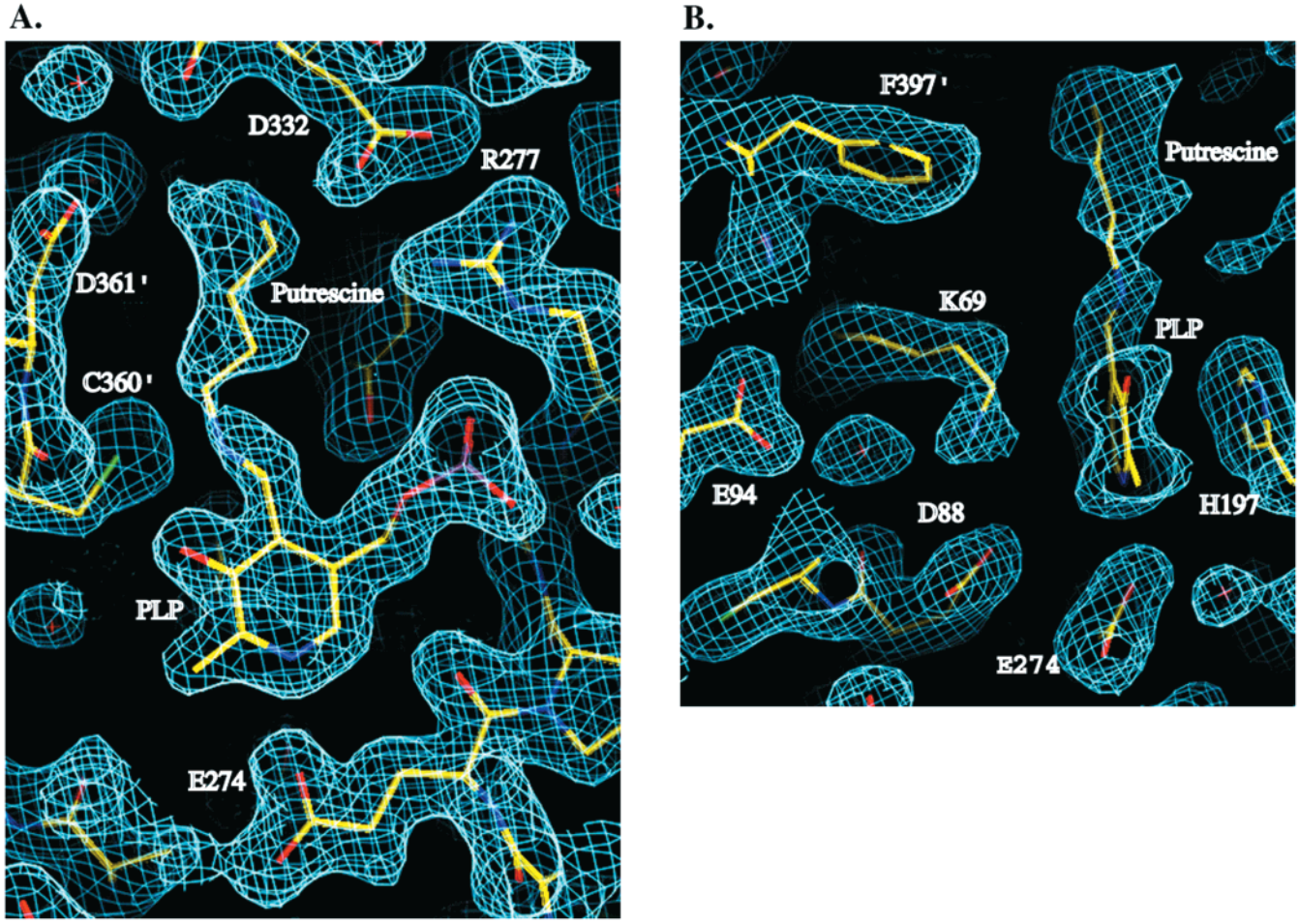

FIGURE 2: Representative electron density for the active site region of the wild-type *T. brucei* ODC structure in complex with putrescine at 2.0 Å. (A) Putrescine binding site and the position of Cys-360 in the putrescine-bound structure. The sulfur of Cys-360 is 3.4 Å from the C_α of putrescine and 4.0 Å from C4′ of PLP. (B) Interactions of Lys-69 in the putrescine-bound structure. The N_Z of Lys-69 is 3.4 Å from O_γ of Asp-88 and is involved in a H-bond network with Glu-94 through an ordered water molecule. The displayed maps are σ_a-weighted $2F_o - F_c$ electron density maps contoured at 0.9 σ and displayed with the program O (*25*). Nitrogen is displayed in blue, oxygen in red, sulfur in yellow, and phosphate in purple. The active site is composed of the N-terminal domain from one subunit and the C-terminal domain of another (distinguished in the figure as residue-number′).

mutant K69A in complex with DFMO (*12*). In the native structure, the side chain of Cys-360 is rotated out of the active site, but in the DFMO-bound structure, the Cys-360 side chain points into the active site, forming a covalent bond with the C_α-methyl group of DFMO. The rotation of Cys-360 into the active site suggests that it may be involved in the chemistry of catalysis; however, because of the covalent nature of the interaction between Cys-360 and DFMO, this structure may not be representative of the position of Cys-360 in the substrate-complexed structure. Further, none of the current structures of any eukaryotic ODC determine the position of Lys-69 in the presence of a bound ligand. To address both questions, we determined the X-ray structure of *T. brucei* ODC bound to putrescine.

Crystals were grown in the presence of D-Orn as described under Experimental Procedures. D-Orn binds *T. brucei* ODC (K_d = 0. 27 mM), but it is not decarboxylated during the time course of a standard assay (2 h at 37 °C, 50 mM D-Orn, 0.01 mM ODC). Data were collected, and the structure was solved by molecular replacement using the *T. brucei* K69A DFMO bound structure as the search model (Table 1). The crystals belong to space group $P2_1$ (a = 67.3 Å, b = 151.6 Å, c = 86.4 Å, β = 103.2°) and diffract to 2.0 Å resolution. Two homodimers occupy the same asymmetric unit. Representative electron density in the active site region of the molecule is displayed in Figure 2. Electron density is observed for the side chain of the bound ligand. Surprisingly, no electron density was observed for the CO_2 moiety of D-Orn, strongly suggesting that D-Orn was decarboxylated in the crystal to form putrescine. While D-Orn is not decarboxylated during the course of a standard assay, the extended time of incubation between D-Orn and enzyme during crystallization allows decarboxylation of the non-physiologic stereoisomer to occur. Thus, this X-ray structure represents the structure of the wild-type enzyme in complex with the product putrescine.

The final model comprises 1496 residues of 4 noncrystallographic symmetry-related *T. brucei* ODC protein chains, 4 PLP, 4 putrescine, and 380 water molecules. The *R*-factor is 23.7% (R_{free} = 28.0%) for 8−2.0 Å resolution ($F > 0\sigma$) data, with the model constrained to preserve noncrystallographic symmetry. When noncrystallographic symmetry constraints were relieved, only slight differences between the subunits were observed. Regions including the N-terminus (residues 1−13), the C-terminus (residues 409−425), and two loops (residues 160−164 and residues 297−311) were disordered, and the density could not be interpreted. However, interpretable electron density was observed for

amino acid residues 14−30 in all monomers and for residues 410−422 in two of the four monomers. These regions of the structure were disordered in both of the previous *T. brucei* ODC structures (*12*). There were indications of double occupancy in the active site, with both putrescine-bound and unliganded molecules contributing to the density. The Lys-69 NZ and putrescine C_α positions have variable electron density in the four active sites. As was observed in the DFMO-bound structure, the side chain moiety of putrescine is in an extended conformation and forms interactions between the δ-amino group of the ligand and two Asp residues (Asp-361 and Asp-332) from different monomers (Figure 2A).

In comparison to the unliganded native structure, only two significant structural rearrangements are observed. First, Cys-360 is rotated toward the active site (Figure 2A), positioning the sulfur to within 3.4 Å of the C_α-carbon of putrescine (it is 6.8 Å away in the native structure). The position of the Cys-360 side chain is similar to that observed in the DFMO-bound structure. Second, Lys-69 swings away from the C4′ atom of PLP, breaking the Schiff base bond to form new interactions with Glu-94 and Asp-88 from the same subunit (Figure 2B). This structural change provides putrescine access to the cofactor to form a Schiff base with PLP in place of Lys-69. These data suggest that Glu-94 and Asp-88 prevent Lys-69 from displacing the substrate during the course of the reaction, explaining why mutation of either residue to Ala decreases the steady-state k_{cat} for the reaction with L-Orn by 30- and 200-fold, respectively (*15*).

UV/Vis Spectral Analysis of C360A and C360S ODC. Similarly to wild-type ODC, C360A and C360S ODC display absorption spectra for the enzyme-bound PLP cofactor with band maxima at 335 and 423 nm (Figure 3), which are characteristic of a Schiff base between Lys-69 and PLP (internal aldimine; Figure 1). The relative intensities of the two bands change with pH, such that the 335 nm band increases, while the 423 nm band decreases with increasing pH. The simplest model that describes the pH titration requires two spectrally distinguishable forms, interconverting with a cooperative $2H^+$ transition, where both groups have the same pK_a (Figure 3 insets). The pK_a's of the titrating group(s) are 8.5 ± 0.1 for C360A ODC and 8.3 ± 0.1 for C360S ODC. These data are nearly identical to the data obtained for the wild-type enzyme (pK_a = 8.7). For the wild-type enzyme, the 423 nm band has been proposed to arise from the PLP species where both the imine nitrogen and the pyridine nitrogen are charged (*16*). Either deprotonation of the pyridine nitrogen or formation of a tetrahedral adduct by addition of a deprotonated nucleophile (e.g., Cys) to the imine double bond could give rise to the 335 nm band at high pH (*16*). Cys-360 would be expected to have a pK_a in the range of the titrating group and is within 3.4 Å of the imine bond. However, the finding that mutation of Cys-360 to Ala or Ser results in the same spectral pH titration as for wild-type ODC suggests that this residue is not involved in the spectral pH titration. Previous analysis of E274A ODC suggested that the spectral change corresponded to loss of the proton on the pyridine nitrogen (*16*).

Steady-State Analysis of C360A and C360S ODC. Steady-state kinetic analysis of the decarboxylation of L-Orn catalyzed by C360A and C360S ODC was followed by measuring CO_2 formation in a coupled enzyme assay in the presence of excess PLP (Experimental Procedures). Mutation of Cys-360 to Ala or to Ser decreases the k_{cat} for the decarboxylation of L-Orn by 50- and 1000-fold, respectively, while the K_m for the reaction decreases by 5−10-fold, such that the effects of the mutations on k_{cat}/K_m are 14- and 130-fold for C360A and C360S ODC, respectively (Table 2). The kinetic term, k_{cat}/K_m, is sensitive to the steps in the reaction up to the first irreversible step, which in this reaction is decarboxylation. Thus, the steady-state data demonstrate that Cys-360 plays a role in facilitating both halves of the reaction, e.g., steps up to and including decarboxylation and those that occur after decarboxylation. Because the effects on k_{cat} are larger than on k_{cat}/K_m, mutation of Cys-360 has a larger effect on steps that occur after decarboxylation. To measure these effects directly, single turnover and pre-steady-state kinetic analyses were performed.

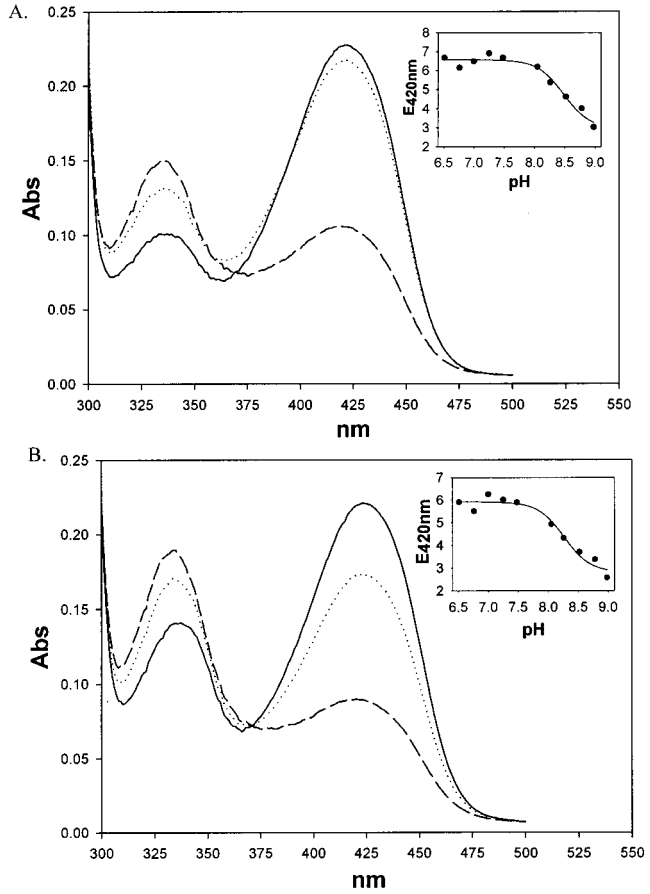

FIGURE 3: Spectral analysis of PLP bound to C360A and C360S ODC. (A) Spectra of C360A ODC (35 μM). (B) Spectra of C360S ODC (35 μM). Spectra were acquired at pH 6.5−9.0 in 0.1 M $NaPO_4$, Hepes, or Bicine and corrected for free PLP using ultrafiltration as described under Experimental Procedures. Representative spectra obtained at pH 7 (line), 8 (dots), and 9 (dashes) are displayed. The insets show the pH dependence of millimolar absorptivities at 420 nm. Data were fitted to eq 1, and the parameters (solid line) calculated from the fit are: for C360A ODC, pK_a = 8.5 ± 0.1, ϵ_{EH} = 6.6 ± 0.1 mM^{-1} cm^{-1}, ϵ_E = 2.9 ± 0.7 mM^{-1} cm^{-1}; for C360S, pK_a = 8.3 ± 0.1, ϵ_{EH} = 5.9 ± 0.2 mM^{-1} cm^{-1}, ϵ_E = 2.8 ± 0.9 mM^{-1} cm^{-1}.

Single Turnover Analysis of the Reaction of C360A, C360S, and Wild-Type ODC with 1-$^{14}CO_2$-L-Orn. The intermediates formed during the reaction of wild-type ODC with L-Orn were previously characterized by stopped-flow multiwavelength spectroscopy (*10*). The data suggested that the decarboxylation step occurred with a rate constant of 20

Table 2: Steady-State and Pre-Steady-State Kinetic Analysis of the Reaction of ODC with L-Orn[a]

enzyme	C360A ODC	C360S ODC	wild-type ODC
	A. Steady-State Decarboxylation		
k_{cat} (s^{-1})	0.27 ± 0.00	0.015 ± 0.000	15 ± 0[b]
K_m (μM)	100 ± 10	54 ± 3	400 ± 10
	B. Multiwavelength Stopped-Flow Analysis		
k_{obs1} (s^{-1})	57 ± 9	25 ± 2	na[c]
k_{obs2} (s^{-1})	11 ± 0	3.0 ± 0.1	na
k_{obs3} (s^{-1})	0.21 ± 0.02	0.049 ± 0.013	na
	C. Single Turnover Analysis		
k_{decarb} (s^{-1})	13 ± 1	2.4 ± 0.5	150 ± 50 (12 ± 1 at 4 °C)
$K_{m.decarb}$ (μM)	570 ± 120	1300 ± 400	570 ± 240 (340 ± 60 at 4 °C)

[a] Data were collected at 37 °C in 0.1 M Hepes, pH 7.5, with the exception that for the single turnover analysis of wild-type ODC, data in parentheses were collected at 4 °C. For sections A and C, reported errors are the standard errors of the fit. For section B, errors are the standard deviation of the mean ($n = 5$ for C360S, $n = 9$ for C360A ODC). [b] Data were taken from (*16*). [c] na: not assessed.

s^{-1}, while the overall rate-limiting step of the reaction was product release, which occurred at 1 s^{-1} (at 4 °C). Both rate constants were estimated to be ~10-fold faster at 37 °C, and at this temperature, Schiff base formation was complete during the dead time of the mixer (<3 ms).

The quantitation of CO_2 formed during the reaction of 1-$^{14}CO_2$-L-Orn with ODC under single turnover conditions ([ODC] ≫ [L-Orn]) measures the kinetics of the reaction steps up to and including decarboxylation. Reaction steps that occur after decarboxylation (C_α-protonation and product release) do not contribute to the observed kinetics in this analysis. The single turnover decarboxylation rate can be limited by the rates of Schiff base formation or by decarboxylation; thus, the method provides an alternate method to measure the minimal rate of the decarboxylation step. The reaction of 1-$^{14}CO_2$-L-Orn with wild-type, C360A, and C360S ODC was followed under single turnover conditions at 37 °C. The single turnover reaction for wild-type ODC was also monitored at 4 °C for comparison to the prior results obtained by stopped-flow multiwavelength spectroscopy. The decay of 1-$^{14}CO_2$ from the reaction solution follows first-order kinetics (Figure 4), and the data were fitted to eq 2A to obtain k_{obs}. The k_{obs} values obtained at different enzyme concentrations were well fit by eq 2B (Figure 4 insets), which describes a one-step binding reaction followed by an irreversible decarboxylation step (Scheme 1). The kinetic parameters (k_{decarb} and $K_{m.decarb}$; Table 2) were determined from the fit. The first-order rate constant, k_{decarb}, represents the rate-limiting step up to and including the decarboxylation step. For wild-type ODC, the single turnover rates at 4 °C are in excellent agreement with the rates of decarboxylation measured in the stopped-flow spectral analysis, confirming the assignment of the rate constant. Compared to the wild-type enzyme, k_{decarb} is decreased by 12- and 65-fold for Cys360A and C360S ODC, respectively. For all three enzymes, k_{decarb} is significantly faster than the overall steady-state rate (k_{cat}), showing that the decarboxylation step is not rate-limiting for either the wild-type or the mutant enzymes.

Pre-Steady-State Analysis of the Reaction of L-*Orn with C360A and C360S ODC by Multiwavelength Stopped-Flow Spectroscopy.* The spectral properties of the PLP cofactor

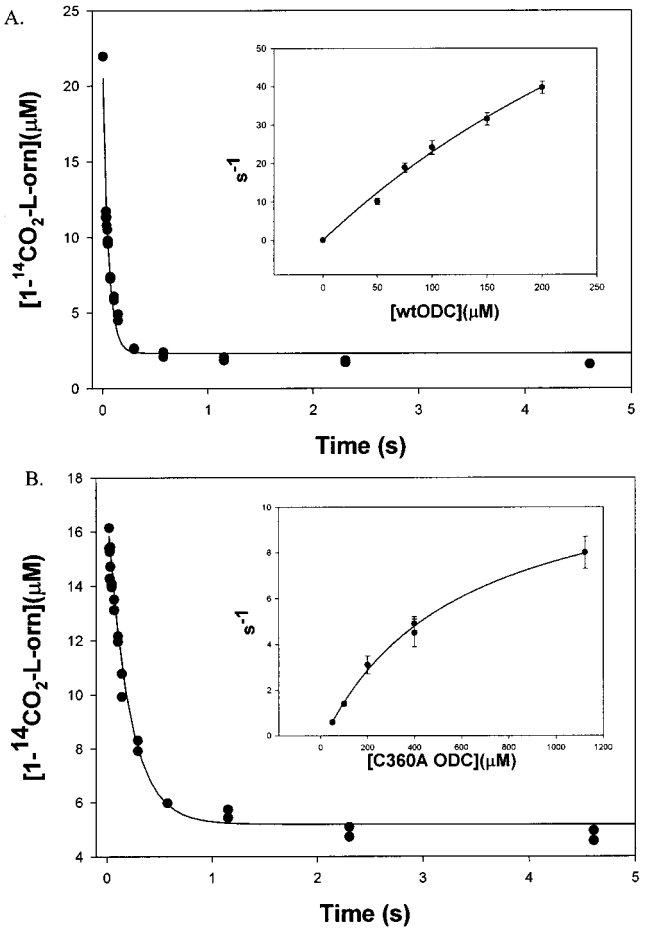

FIGURE 4: Single turnover analysis of L-Orn decarboxylation by ODC. 1-$^{14}CO_2$-L-Orn (17 μM) was incubated with a molar excess of ODC. (A) Wild-type ODC (0.075 mM). (B) C360A ODC (0.4 mM). Reactions were performed in 0.1 M Hepes, pH 7.5, at 37 °C. Reactions were quenched with an equal volume of 2 M NaOH and 50 mM cold L-Orn, followed by acidification of the mixture to drive CO_2 from solution. The concentration of L-Orn remaining after the reaction is plotted vs the incubation time of the reaction. Data were fitted to eq 2A to obtain k_{obs} (solid lines). Insets show a plot of k_{obs} vs the concentration of enzyme, where the solid lines represent the fits to eq 2B. Error bars represent the standard error of the fit to eq 2A. The kinetic parameters (k_{decarb} and $K_{m.decarb}$) obtained from the fit to eq 2B are displayed in Table 2.

are sensitive to the electronic and tautomeric state of the cofactor providing a mechanism to monitor the formation and decay of key reaction intermediates. The reactions of C360A and C360S ODC with L-Orn (10 mM) were followed by multiwavelength stopped-flow spectroscopy at 37 °C (Figure 5). For both mutant enzymes, three kinetic phases are observed. The first phase is characterized by an increase in absorbance at 423 nm. This phase is followed by a decrease in the absorbance at 423 nm, concomitant with an increase in absorbance at 335 nm. The final slow phase is characterized by a continued decrease in absorbance at 423 nm for both mutants. For C360A ODC, a blue shift in the 335 nm band is also observed in the final stages of the reaction, while for C360S ODC a decrease in absorbance at 335 nm is observed. In addition for C360A ODC, the 423 nm peak is asymmetric at some of the intermediate time points, suggesting that multiple species may contribute to the spectra. In contrast, for C360S ODC the bands at both 335 and 423 nm are symmetric at all time points.

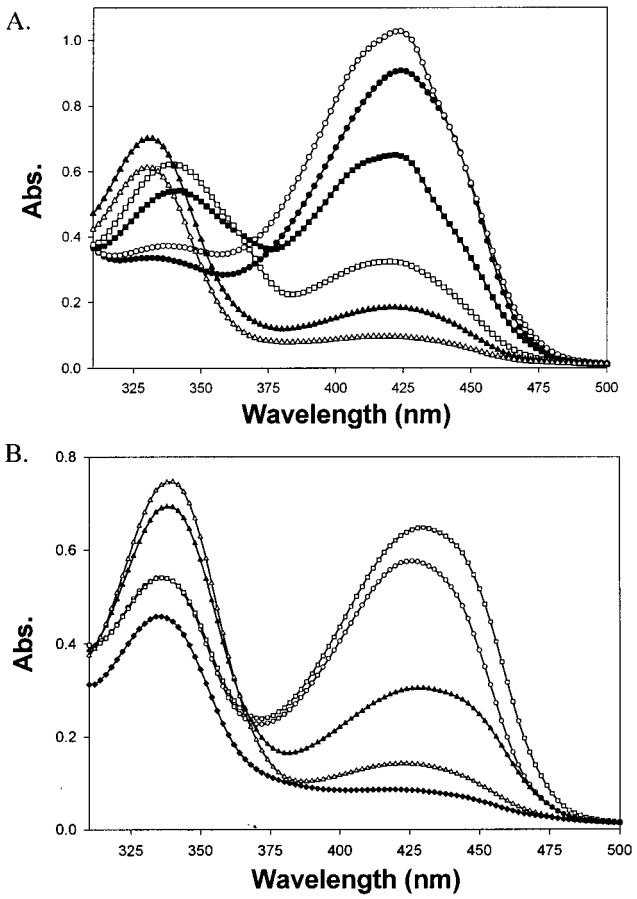

FIGURE 5: Multiwavelength stopped-flow analysis of the reactions of L-Orn with C360A ODC. (A) Representative absorbance spectra of C360A ODC (0.12 mM) at selected time points after mixing with L-Orn (10 mM) in 0.1 M Hepes, pH 7.5, at 37 °C. Spectra 4 ms after mixing (●), spectra 24 ms after mixing (○), spectra 120 ms after mixing (■), spectra 690 ms after mixing (□), spectra 7 s after mixing (▲), spectra 58 s after mixing (△). (B) Representative absorbance spectra of C360S ODC (0.12 mM) at selected time points after mixing with L-Orn (10 mM) in 0.1 M Hepes, pH 7.5, at 37 °C. Spectra 3 ms after mixing (○), spectra 50 ms after mixing (□), spectra 450 ms after mixing (▲), spectra 1506 ms after mixing (△), spectra 58 s after mixing (◆).

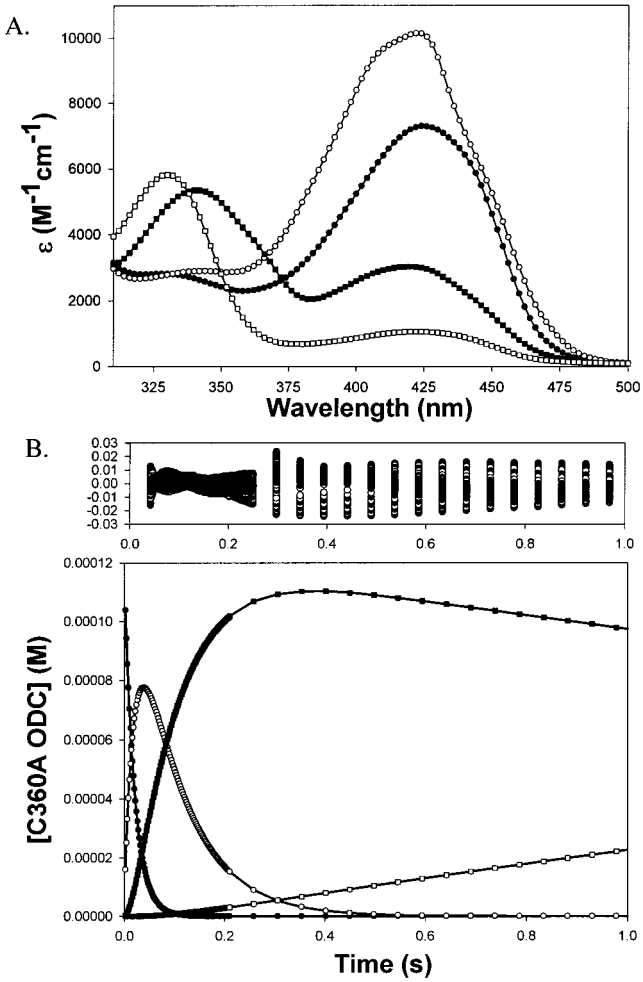

FIGURE 6: Global kinetic analysis of the multiwavelength stopped-flow data for C360A ODC. Data were fit by global kinetic analysis to the equation describing a three-step sequential reaction model (Scheme 2), where four species [A (●), B (○), C (■), and D (□)] are interconverted by three rate constants (k_{obs1}, k_{obs2}, k_{obs3}). The values for the fitted parameters are displayed in Table 2. (A) Model-derived wavelength dependence of the extinction coefficients. (B) Model-derived concentration profiles. The residuals to the fit of the absorbance data are displayed above panel B as Abs vs time. The standard errors of the fits of absorbance data to the model were calculated for C360A ODC ($\sigma = 0.012 \pm 0.004$) or C360S ODC ($\sigma = 0.0044 \pm 0.0023$), where the error is the standard deviation of the mean for $n = 9$ and $n = 5$ separate shots.

Global kinetic analysis of the multiwavelength data (310−500 nm) was performed as described under Experimental Procedures. The data were well fit by a three-step sequential model (Scheme 2) in which intermediates A−D form and decay as described by three rate constants (k_{obs1}, k_{obs2}, k_{obs3}). The model-derived spectra of the intermediates for C360A ODC are displayed in Figure 6. The analysis produced similar results for the C360A and C360S mutants, except that the species arise at different rates in the two mutants. The analysis was not able to resolve any additional species in the case of C360A ODC, despite the asymmetric nature of some of the spectra. The spectra of intermediates A and B are characteristic of either the internal or the external aldimine species (Figure 1), suggesting that A represents the internal aldimine with Lys-69 (starting spectra), that B represents the external aldimine with L-Orn, and that Schiff base formation is described by k_{obs1}. The spectra of intermediates C and D are characterized by an intense band at 335 nm, with little to no 423 nm band character. Spectral analysis of PLP-dependent aminotransferases [e.g., aspartate aminotransferase (*33*)] demonstrates that these spectra are characteristic either of a ketimine intermediate or of PMP. A spectral species consistent with PMP is not formed upon similar incubation of these mutant enzymes with putrescine, suggesting that a decarboxylation-dependent transamination is catalyzed by the mutant enzymes. These results are consistent with a reaction in which the quinoid intermediate is incorrectly protonated on C4′ instead of at C_α, to produce the ketimine intermediate, followed by Schiff base hydrolysis/product release to form PMP and γABA (Figure 1). For both mutant enzymes, the magnitude of k_{obs2} is the same as k_{decarb} measured by single turnover analysis, while k_{obs3} is similar in magnitude to k_{cat} obtained by steady-state analysis (Table 2). These data suggest that k_{obs2} represents the decarboxylation/protonation steps to form ketimine and that k_{obs3} represents product release (which is likely to be dominated by Schiff base hydrolysis) to form PMP and γABA.

Product Analysis of the Steady-State Reaction of L-*Orn with Wild-Type, C360A, and C360S ODC by HPLC.* To confirm that the formation of the 335 nm absorption band during the reaction with L-Orn results from a decarboxylation-dependent transamination event, the reaction products were analyzed by HPLC after derivatization using the AccQ·TAG kit (Waters, Milford, MA). The AccQ·TAG column was calibrated using known concentrations of derivatized L-Orn, putrescine, and pyrrolidine. If L-Orn undergoes both decarboxylation and transamination, the expected product is γABA. While no good commercial source of γABA exists to serve to standardize the column, reduction of γABA with $NaBH_4$ produces pyrrolidine (Figure 1B), which is commercially available. Thus, reaction products were analyzed both before and after $NaBH_4$ reduction, and pyrrolidine was used as a standard for the decarboxylation-dependent transamination reaction. The analysis provided good chromatographic separation of all major substrate and product species, allowing the rates of formation of putrescine, PMP, pyrrolidine, and γABA to be determined. Cadaverine was added to all samples as an internal standard for quantitation. The reaction of ODC with L-Orn (2 mM) was carried out in the presence of excess free PLP (0.2−2 mM) so that PMP formed during the reaction could be exchanged for free PLP to restore the catalytically competent form of the enzyme.

For wild-type ODC, the reaction with L-Orn produced putrescine (Figure 7A). A small peak is observed at the retention time of pyrrolidine in the $NaBH_4$ reduced sample. However, this peak was also present in control samples containing putrescine and the other assay components without enzyme. There is no evidence for PMP or γABA formation in any of the wild-type samples. In contrast, for C360A ODC, two additional peaks are observed in the $NaBH_4$ reduced sample corresponding to pyrrolidine and to PMP (Figure 7B). In the nonreduced sample, a novel peak is present with a retention time of 12.5 min. This peak disappears upon reduction, allowing the peak to be assigned to γABA. Similar results were obtained for C360S ODC (data not shown).

The rates of product formation were determined using the HPLC assay (Table 3). For steady-state analysis of the reaction rates, the reactions were followed for multiple turnovers (25−250 for C360A; 20−100 for C360S ODC; 200−600 for wild-type ODC) corresponding to depletion of no more than 25% of either L-Orn or PLP during the reaction. At longer incubation times, both C360A and C360S ODC were capable of driving the near-complete conversion of PLP to PMP. Thus, PMP readily exchanges with PLP to allow multiple turnovers of the reaction, consistent with the finding that the affinity of the enzyme for PMP is weaker than for PLP (*16*). In short, PLP functions as a substrate in the reaction catalyzed by the mutant enzymes. For wild-type ODC, the rate of putrescine formation is in excellent agreement with the rate of steady-state decarboxylation (Table 2). For C360A and C360S ODC, putrescine formation accounts for only 10% of total product formation, while γABA, quantitated by γABA in the nonreduced samples or by pyrroldine in the reduced samples, accounts for 90%. The rate of PMP formation is similar to the rate of γABA formation. These data demonstrate that for the mutant enzymes 90% of the substrate that is decarboxylated goes on to be transaminated. The rates of product formation catalyzed by C360S ODC are about 10-fold slower than for C360A ODC; however, the product ratios (putrescine/γABA) are similar for the two mutant enzymes.

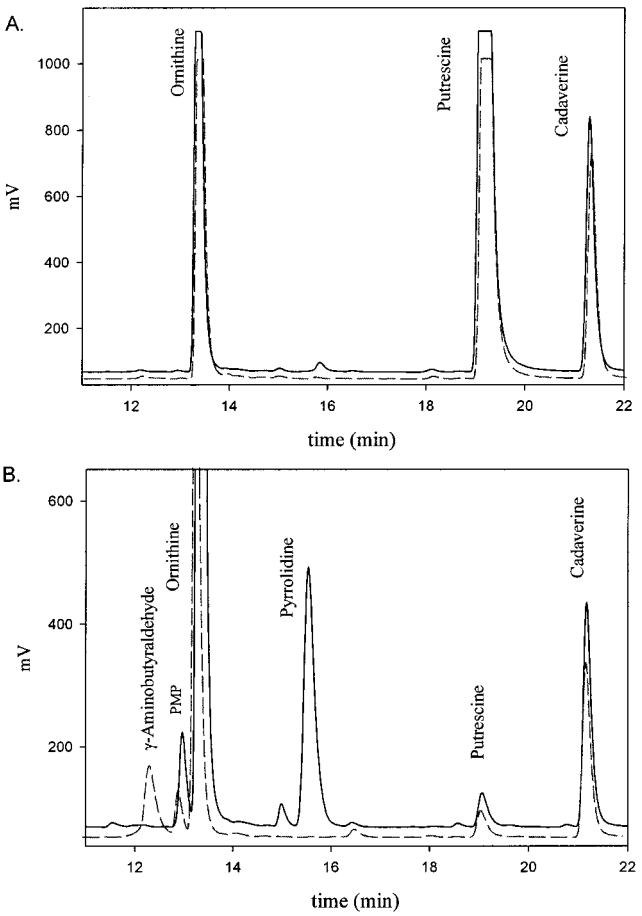

FIGURE 7: HPLC analysis of the reaction products formed upon incubation of wild-type and C360A ODC with L-Orn. Representative samples are displayed in which 25% of the L-Orn was consumed during the reaction time. (A) Wild-type ODC (0.25 μM) was incubated with L-Orn (2 mM) and PLP (1 mM) for 360 s. (B) C360A ODC (2.5 μM) was incubated with L-Orn (2 mM) and PLP (2 mM) for 960 s. The reactions were quenched with TCA, and cadaverine was added as an internal standard. Part of the reaction was treated with $NaBH_4$. Products were derivatized and analyzed on an AccTag column as described under Experimental Procedures. The retention times of control reagents were used to identify the peaks, which are labeled on the chromatograms [plot of mV recorded on the detector vs retention time (min)]. Solid lines represent the reduced samples, and dashed lines represent the nonreduced samples.

Table 3: Product Analysis of the Reaction of ODC with L-Orn As Determined by HPLC Analysis[a]

enzyme	k_{cat}(Put) (s^{-1})	k_{cat}(γABA) (s^{-1})	k_{cat}(PMP) (s^{-1})	k_{cat}(total) (s^{-1})
C360A ODC	0.019 ± 0.005	0.22 ± 0.02	0.16 ± 0.03	0.24
C360S ODC	0.0025 ± 0.0006	0.028 ± 0.01	0.022 ± 0.002	0.031
wild-type ODC	11 ± 2	nd	nd	11

[a] Assays were performed in 15 mM potassium phosphate, pH 7.4, at 37 °C. nd: not detectable. The total k_{cat} represents the total rate of L-Orn decarboxylation and is the sum of the rates of putrescine (Put) and γABA formation. Errors are the standard deviation of the mean where $n = 4$.

For wild-type ODC, decarboxylation-dependent transamination could not be detected by the HPLC assay. However, in the presence of a large excess of substrate (L-Orn = 250 mM), which allows the reaction to be followed for many

turnovers, conversion of PLP to PMP could be detected by following the absorbance change of the cofactor at 420 nm. The rate of PMP formation was determined during the steady-state phase of this reaction. For wild-type ODC, decarboxylation-dependent transamination occurs in only $1/10^4$ catalytic events ($k_{transam} = 0.001\ s^{-1}$). Thus, for C360A ODC, the rates of the transamination side reaction (Table 3) have increased by 200- and 30-fold, while the rates of the on-pathway reaction to produce putrescine have decreased by 600- and 4000-fold for C360A and C360S ODC, respectively.

DISCUSSION

The PLP cofactor is inherently capable of catalyzing a wide range of reactions, including decarboxylation, racemization, and transamination of L-amino acids. The reaction specificity of a PLP-dependent enzyme is therefore dictated by the specific nature of the enzyme active site, which promotes the physiological reaction, while discouraging potential side reactions. As has been reported for other PLP-dependent decarboxylases (*6*−*8*), wild-type *T. brucei* ODC is capable of a very high level of reaction fidelity. The enzyme promotes decarboxylation of L-Orn to produce putrescine almost exclusively. The one observed side reaction, decarboxylation-dependent transamination to produce γ-aminobutyaldehyde (γABA) and PMP, occurs at a rate that is approximately 10^4-fold slower than the preferred reaction.

In contrast to the high level of reaction specificity that is achieved during catalysis by wild-type ODC, mutation of the active site residue Cys-360 to either Ala or Ser converts ODC into a decarboxylation-dependent transaminase. For the reaction of the C360A and C360S mutant enzymes with L-Orn, γABA represents 90% of the product that is formed, while putrescine is produced in only 10% of the catalytic events. This change in reaction specificity is a result of both an increase in the rate of the side reaction to produce γABA (200-fold for C360A and 30-fold for C360S) and a decrease in the observed rate of putrescine formation (600-fold for C360A and 4000-fold for C360S). γABA formation would be promoted along the reaction pathway if the decarboxylated substrate (quinoid) intermediate is protonated at C4′ instead of at C_α (Figure 1). Mutation of Cys-360 allows protonation of C4′ by H_2O (or another acid in the active site) to compete effectively with the reaction at C_α. Thus, the mutant enzyme remains capable of selectively cleaving the correct bond between C_α and CO_2, but is incapable of correctly performing the protonation reaction. The X-ray structure of *T. brucei* ODC bound to putrescine demonstrates that the Cys-360 side chain rotates into the active site upon ligand binding, positioning the sulfur to within 3.4 Å of the C_α-carbon. These data are consistent with a role for Cys-360 as a general acid to guide correct protonation of the decarboxylated reaction intermediate at C_α. The finding that Ser, which has a similar size to Cys but a much higher pK_a, is unable to replace the function of Cys is also consistent with this hypothesis. A Cys residue has recently been shown to serve as a general acid in the reaction catalyzed by *T. cruzi S*-adenosylmethionine decarboxylase, contributing specifically to the steps involved in Schiff base formation and hydrolysis (*34*). However, the high pK_a of the hydroxyl group may not be the only factor affecting the ability of the Ser side chain to replace the function of the Cys residue. The Ser side chain may also be unable to fully rotate into the active site. As an alternative to functioning as a general acid, Cys-360 may serve to inhibit access of water to the C4′ atom, thereby preventing the transamination side reaction.

For wild-type ODC, the rate of the decarboxylation step had previously been assessed by multiwavelength stopped-flow analysis at 4 °C (*10*). Measurement of the decarboxylation reaction under single turnover conditions provides an alternate method to determine the minimal rate of the decarboxylation step. For wild-type ODC, the decarboxylation rate measured in the single turnover reaction (Table 2) is in excellent agreement with the rate of decarboxylation determined by stopped-flow spectroscopy (*10*), confirming the assignment of the observed spectral change to the decarboxylation step. For the C360A and C360S mutant enzymes, the rate of single turnover decarboxylation reaction decreased by 12- and 65-fold, respectively, in comparison to the wild-type enzyme. This rate could be limited either by Schiff base formation or by the decarboxylation step. However, like the wild-type enzyme, the multiwavelength stopped-flow data (below) suggest that Schiff base formation is faster than the single turnover decarboxylation rate and, thus, the method provides a measure of the decarboxylation step. Furthermore the observed carbon-13 isotope effect for C360A ODC was near the intrinsic level, suggesting that the decarboxylation step occurs at a slower rate than Schiff base interchange (*35*). Therefore, Cys-360 plays a role in facilitating decarboxylation.

Global kinetic analysis of the pre-steady-state spectral data for the reaction of L-Orn with C360A and C360S ODC demonstrates that both reactions are well fit by a simple three-step sequential model (Scheme 2). The model-derived spectral characteristics of the intermediates are consistent with a reaction mechanism in which formation of the external aldimine (species B) occurs with a rate constant of k_{obs1} (Table 2). This step is followed by slower formation of the ketimine intermediate (species C) with a rate constant of k_{obs2} and by formation of products (species D) with a rate of k_{obs3} (Table 2). For wild-type ODC, Schiff base formation with L-Orn occurs in the dead time of the mixer ($>500\ s^{-1}$ at 37 °C). The mutations at C360 slow the rate of this step (k_{obs1}) by at least 10-fold. These data suggest a role for Cys-360 in the acid/base chemistry of Schiff base formation. In the next step, ketimine formation (species C) occurs at the same rate as the single turnover decarboxylation step for both mutant enzymes ($k_{obs2} = k_{decarb}$), providing strong evidence that the rate-limiting step in ketimine formation is decarboxylation. Thus, either protonation at C4′ to form the ketimine intermediate must occur in a concerted reaction with decarboxylation, or the rate of the protonation step is very fast in comparison.

Finally, the magnitude of k_{obs3} is very similar to the steady-state k_{cat} measured for both mutant enzymes, suggesting that this step represents Schiff base hydrolysis to form the products, PMP and γABA, or the rate of release of one of the two products. Thus, as for wild-type ODC, Schiff base hydrolysis/product release remains the rate-limiting step; however, the rate of this step has been slowed significantly. This finding is not surprising considering that the acid/base chemistry of the enzyme active site is optimized to cleave a Schiff base bond between the α-amino group and C4′ and not to cleave the bond between the α-amino group and C_α.

In support, carbon-13 isotope data suggest that the off-rate of L-Orn was not altered by the mutation. For wild-type ODC, the carbon-13 isotope data ($^{12}k/^{13}k = 1.033$) suggest that the rate of the decarboxylation step is similar to the rate of Schiff base hydrolysis to release L-Orn (*35*). For C360A, the decarboxylation rate has been slowed by 12-fold in comparison to the wild-type enzyme, yet the carbon-13 isotope effect ($^{12}k/^{13}k = 1.0525$) is near the intrinsic limit. Since the decarboxylation rate is only 12-fold slower in the mutant enzyme, any slow-down in the off-rate of L-Orn relative to wild-type ODC would have been expected to suppress the isotope effect below the intrinsic limit.

In summary, Cys-360 has a catalytic role in three of the essential reaction steps catalyzed by ODC: Schiff base formation, decarboxylation, and protonation. Analysis of the kinetic mechanism of the K69R mutant *T. brucei* ODC demonstrated that Lys-69 also played multiple roles in the catalytic mechanism, catalyzing Schiff base formation, Schiff base hydrolysis, and decarboxylation (*14*). Thus, it appears likely that the ODC active site has been optimized to utilize active site residues in multiple roles, suggesting that the catalytic residues in the active site act synergistically to stabilize the multiple transition states formed during the reaction pathway.

Despite the fact that the PLP cofactor is capable of catalyzing such diverse chemistry, few mutagenesis experiments that alter reaction specificity, as opposed to substrate specificity, have been reported. Aspartate aminotransferase was converted by three active site mutations into a β-decarboxylase, a reaction that is not catalyzed to a significant extent by the wild-type enzyme (*36*). The change in reaction specificity occurred as a result of both an increase in the novel decarboxylase activity and a decrease in the physiological transaminase activity. Likewise, the change in reaction specificity for C360A and C360S ODC occurrs both because of an increase in the rate of the side reaction transamination and because of a decrease in the rate of the physiological reaction. Engineering novel reaction specificity into PLP-dependent enzymes will require a thorough understanding of the structural features in the active sites that control this specificity. To understand the structural basis for the reaction specificity in ODC, two steps need to be considered: (1) How does the enzyme control bond cleavage to the C_α-carbon, and (2) how does the enzyme control the protonation of the decarboxylated reaction intermediate to form putrescine? These data demonstrate that Cys-360 is a major determinant in the control of the protonation step. Finally, mutation of Cys-360 provides a strategy for creating a novel transaminase activity in this class of PLP-dependent enzymes.

ACKNOWLEDGMENT

We are grateful to L. Esser for helping with the X-ray data collection and for sharing his expertise on structure refinement, and to S. Ye and N. Grishin for their help during the structure refinement. We also thank K. Henderson and T. Earnest at the Advanced Light Source beam line 5.0.2 for help with data collection.

REFERENCES

1. Phillips, M. A. (1999) Ornithine decaboxylase. in *The encyclopedia of molecular biology* (Creighton, T., Ed.) pp 1726−1730, John Wiley & Sons, New York.
2. Marton, L. J., and Pegg, A. E. (1995) *Annu. Rev. Pharmacol. Toxicol. 35*, 55−91.
3. Wang, C. C. (1995) *Annu. Rev. Pharmacol. Toxicol. 35*, 93−127.
4. John, R. A. (1995) *Biochim. Biophys. Acta 1248*, 81−96.
5. Grishin, N. V., Phillips, M. A., and Goldsmith, E. J. (1995) *Protein Sci. 4*, 1291−1304.
6. Stevenson, D. E., Akhtar, M., and Gani, D. (1990) *Biochemistry 29*, 7631−7647.
7. Akhtar, M., Stevenson, D. E., and Gani, D. (1990) *Biochemistry 29*, 7648−7660.
8. Choi, S. Y., and Churchich, J. E. (1986) *Eur. J. Biochem. 160*, 515−520.
9. Dunathan, H. C. (1966) *Proc. Natl. Acad. Sci. U.S.A. 55*, 712−716.
10. Brooks, H. B., and Phillips, M. A. (1997) *Biochemistry 36*, 15147−15155.
11. Kern, A. D., Oliveira, M. A., Coffino, P., and Hackert, M. (1999) *Structure 7*, 567−581.
12. Grishin, N. V., Osterman, A. L., Brooks, H. B., Phillips, M. A., and Goldsmith, E. J. (1999) *Biochemistry 38*, 15174−15184.
13. Almrud, J. J., Oliveira, M. A., Grishin, N. V., Phillips, M. A., and Hackert, M. L. (2000) *J. Mol. Biol. 295*, 7−16.
14. Osterman, A. L., Brooks, H. B., Jackson, L., Abbott, J. J., and Phillips, M. A. (1999) *Biochemistry 38*, 11814−11826.
15. Osterman, A., Kinch, L. N., Grishin, N. V., and Phillips, M. A. (1995) *J. Biol. Chem. 270*, 11797−11802.
16. Osterman, A. L., Brooks, H. B., Rizo, J., and Phillips, M. A. (1997) *Biochemistry 36*, 4558−4567.
17. Poulin, R., Lu, L., Ackermann, B., Bey, P., and Pegg, A. E. (1992) *J. Biol. Chem. 267*, 150−158.
18. Coleman, C. S., Stanley, B. A., and Pegg, A. E. (1993) *J. Biol. Chem. 268*, 24572−24579.
19. Tsirka, S., and Coffino, P. (1992) *J. Biol. Chem. 267*, 23057−23062.
20. Osterman, A. L., Grishin, N. V., Kinch, L. N., and Phillips, M. A. (1994) *Biochemistry 33*, 13662−13667.
21. Kunkel, T. A. (1985) *Proc. Natl. Acad. Sci. U.S.A. 82*, 488.
22. Grishin, N. V., Osterman, A. L., Goldsmith, E. J., and Phillips, M. A. (1996) *Proteins: Struct., Funct., Genet. 24*, 272−273.
23. Otwinowski, Z. (1993) *Ocillation data reduction program. Data collection and processing* (Sawyer, L., Isaacs, N., and Bailey, S., Eds.) pp 56−62, Science and Engineering Council, U.K.
24. Navaza, J. (1994) *Acta Crystallogr. A50*, 157−163.
25. Jones, T. A., and Kjeldgaard, M. (1991) *O version 5.4*, Uppsala University, Sweden.
26. Adams, P. D., Pannu, N. S., Read, R. J., and Brunger, A. T. (1997) *Proc. Natl. Acad. Sci. U.S.A. 94*, 5018−5023.
27. Brunger, A. T. (1992) *Nature 355*, 472−474.
28. Pannu, N. S., and Read, R. J. (1996) *Acta Crystallogr. A52*, 659−668.
29. Laskowski, R. A., MacArthur, M. W., Moss, D. S., and Thornton, J. M. (1993) *J. Appl. Crystallogr. 26*, 283−291.
30. Hiromi, K. (1979) *Kinetics of Fast Reactions* (Hiromi, K., Ed.) Halsted Press, New York.
31. Malinowski, E. R. (1991) *Factor analysis in chemistry* (Malinowski, E., Ed.) John Wiley & Sons Inc., New York.
32. Stultz, L. K., Binstead, R. A., Reynolds, M. S., and Meyer, T. J. (1995) *J. Am. Chem. Soc. 117*, 2520−2532.
33. Goldberg, J. M., and Kirsch, J. F. (1996) *Biochemistry 35*, 5280−5291.
34. Kinch, L. N., and Phillips, M. A. (1999) *Biochemistry*.
35. Swanson, T., Brooks, H. B., Osterman, A. L., O'Leary, M., and Phillips, M. A. (1998) *Biochemistry 37*, 14943−14947.
36. Graber, R., Kasper, P., Malashkevich, N., Strop, P., Gehring, H., Jansonius, J. N., and Christen, P. (1999) *J. Biol. Chem. 274*, 31203−31208.

BI001209S